Least energy trajectory generation for quadrotors using rotor acceleration as control inputs

Paraj Ganchaudhuri and Chayan Bhawal

Abstract— **Quadrotors hold significant promise for aerial transportation but are constrained by high energy demands and limited battery capacity. Energy-efficient trajectory planning, based on physics-based models, offers a practical alternative when hardware optimization is not feasible. However, existing formulations often model thrust and torque as inputs, leading to trajectories that are difficult to realize in practice. In this work, we reformulate the optimal control problem by using rotor accelerations as control inputs and allowing an open final time, enabling a balance between hover and propulsion energy. Practical constraints on rotor speeds and accelerations are explicitly incorporated, resulting in feasible, least-energy trajectories. Through numerical simulations, we further demonstrate how optimizing rotor parameters can significantly reduce the total energy consumption.**

Keywords: **Quadrotor, Energy efficient path planning, Optimal control problem, Optimization.**

I. INTRODUCTION

Quadrotors are increasingly recognized as promising platforms for transportation due to their agility, compactness, and ease of control [1]–[3]. However, limited flight endurance—constrained by fixed-capacity batteries [4] and the significant energy demands for lift—remains a major challenge [5]. Efforts to enhance energy efficiency typically focus on hardware optimization, energy-efficient trajectory planning, or multi-agent operations [6].

When hardware redesign or multi-agent operations are not feasible, energy-efficient trajectory planning offers a practical alternative [3], [4], [7]. A widely adopted strategy for energy-efficient planning is the formulation of an optimal control problem (OCP). The first step in constructing an OCP is the development of an accurate energy consumption model (ECM) [8], a task that remains challenging [2]. Various ECM types exist—namely aerodynamic-based models, physics-based models, and black-box models [3]. In this work, we adopt a physics-based model, following [7], as it explicitly accounts for forces and torques acting on the quadrotor for energy computation.

Several studies have investigated least-energy path planning using physics-based models [4], [7]. However, notable gaps remain, which this work aims to address. Most existing formulations model the system dynamics with thrust and torques as inputs, a framework that can yield solutions that are impractical for real-world implementation (Section III-C). We demonstrate that by embedding the state space into a higher-dimensional vector space and utilizing rotor accelerations as control inputs, these limitations can be effectively mitigated (Section III-B).

Even in works where rotor acceleration is used as the control input, the mission completion time is typically fixed [4], [7]. Since quadrotors continuously expend hover energy to generate lift and propulsion energy during movement, there exists an inherent trade-off: flying slowly reduces propulsion energy

but increases hover time, while flying faster shortens hover duration but raises propulsion costs. Therefore, determining an optimal mission time is crucial to balance these competing energy components effectively.

A notable study addressing least-energy trajectory optimization with an open final time is presented in [9]; however, it is restricted to two-dimensional motion. A related work [10] extends the framework to three-dimensional trajectories with open final time, using a physics-based model. Nevertheless, it formulates the OCP with thrusts and torques as inputs and does not incorporate practical constraints on rotor speeds and accelerations, potentially leading to infeasible solutions (see Section III-C). In contrast, our approach explicitly integrates these constraints into the problem formulation (see Section III), ensuring practical, feasible, and energy-efficient trajectories.

As a whole, while some works adopt rotor acceleration as control inputs but assume a fixed mission time [4], [7], and others optimize over an open final time but use thrust and torques as inputs [9], [10], our formulation combines both features: rotor acceleration as control inputs and an open final time. This integration ensures both physical feasibility and optimal energy efficiency.

The rest of the paper is organized as follows: In Section II, we describe the dynamics of quadrotor motion and present the ECM. Section III is dedicated to formulating the OCP, accompanied by numerical simulations, a comparison with an alternate OCP from the literature and an analysis on the role of rotor parameters in optimal energy consumption. Finally, we provide the concluding remarks in Section IV.

II. PRELIMINARIES

In this section, we present a brief overview of a quadrotor's equations of motion and its propulsion dynamics. These notions will be the basis of the OCP formulated to solve the problem at hand.

A. Notations

$\mathbb{R}^n$	Set of $n \times 1$ vectors with real elements.
$\mathbb{R}_+$	Set of real non-negative numbers.
$\mathbb{R}_+^n$	Set of $n \times 1$ vectors with elements from $\mathbb{R}_+$.
$\mathbf{0}_{i \times j}$	$i \times j$ matrix with all elements zero.
$\mathbf{I}_n$	$n \times n$ identity matrix.
$\mathbf{1}_n$	$1 \times n$ vector with all elements one.
$A \otimes B$	Kronecker product of matrices A and B.
$x_i(t)$	i^{th} state of a quadrotor.
$\mathtt{L}_p, \mathtt{U}_p$	Lower and upper limits of variable p.
$\mathbb{M}$	Mission by a quadrotor (see Definition (1)).
$\mathbb{E}_{\mathbb{M}}$	Energy consumed by quadrotor to complete $\mathbb{M}$.
t_i, t_f	Initial and final time, respectively.
$t_{\mathbb{M}}$	Time taken by quadrotor to complete $\mathbb{M}$.
p^*	Optimal variable p.
m, d	Quadrotor mass $[kg]$ and arm length $[m]$.
g	Acceleration due to gravity $[m/s^2]$.
$\mathbb{I}_i$	Inertia along i^{th} direction $[kgm^2]$.
$\kappa_{\mathrm{T}}, \kappa_\tau$	Thrust and torque co-efficient, respectively.

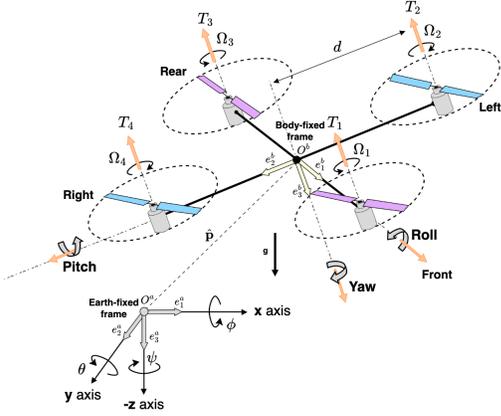|	
$\Omega_i(t)$	Angular velocity of ith rotor shaft $[rad/s]$.
$\alpha_i(t)$	Angular acceleration of ith rotor shaft $[rad/s^2]$.
J	Moment of inertia of motor & propeller $[kgm^2]$.
ϕ, θ, ψ	Roll, pitch, yaw angle of a quadrotor with respect to earth-frame of reference $[rad]$.
$p_{\mathbf{x}}, p_{\mathbf{y}}, p_{\mathbf{z}}$	Absolute position of a quadrotor along $\mathbf{x}$, $\mathbf{y}$, $\mathbf{z}$ direction in earth-frame of reference $[m]$.
$\tau_\phi, \tau_\theta, \tau_\psi$	Roll torque, pitch torque, yaw torque $[Nm]$.

Fig. 1: Schematic of a quadrotor

B. Equation of quadrotor dynamics

A quadrotor (shown in Fig. 1) maneuvers itself in 3D space by variation in thrusts and torques produced by various combination of rotor speeds among its four rotors (motor-propeller pair). The thrust T_i produced by rotor i ($i \in \{1,2,3,4\}$) varies with rotor speed ω_i as $T_i = \kappa_T \omega_i^2$ [7], [10]. The net thrust (T) and net torques ($\tau_\phi, \tau_\theta, \tau_\psi$) are related to rotor speeds by the following equations Eq. (1) and Eq. (2):

$$\underbrace{\begin{bmatrix} T \\ \tau_\phi \\ \tau_\theta \\ \tau_\psi \end{bmatrix}}_{\mathbb{T}} = \underbrace{\begin{bmatrix} \kappa_T & \kappa_T & \kappa_T & \kappa_T \\ 0 & -d \times \kappa_T & 0 & d \times \kappa_T \\ -d \times \kappa_T & 0 & d \times \kappa_T & 0 \\ \kappa_\tau & -\kappa_\tau & \kappa_\tau & -\kappa_\tau \end{bmatrix}}_{\Lambda^{-1}} \underbrace{\begin{bmatrix} \omega_1^2 \\ \omega_2^2 \\ \omega_3^2 \\ \omega_4^2 \end{bmatrix}}_{\omega} \quad (1)$$

$$\underbrace{\begin{bmatrix} \omega_1 \\ \omega_2 \\ \omega_3 \\ \omega_4 \end{bmatrix}}_{\omega} = \sqrt{\underbrace{\begin{bmatrix} \frac{1}{4\kappa_T} & 0 & -\frac{1}{2d \times \kappa_T} & \frac{1}{4\kappa_\tau} \\ \frac{1}{4\kappa_T} & -\frac{1}{2d \times \kappa_T} & 0 & -\frac{1}{4\kappa_\tau} \\ \frac{1}{4\kappa_T} & 0 & \frac{1}{2d \times \kappa_T} & \frac{1}{4\kappa_\tau} \\ \frac{1}{4\kappa_T} & \frac{1}{2d \times \kappa_T} & 0 & -\frac{1}{4\kappa_\tau} \end{bmatrix}}_{\Lambda} \underbrace{\begin{bmatrix} T \\ \tau_\phi \\ \tau_\theta \\ \tau_\psi \end{bmatrix}}_{\mathbb{T}}} \quad (2)$$

Defining $\mathbf{c}_\bullet := \cos(\bullet), \mathbf{s}_\bullet := \sin(\bullet)$, the inertia ratios as $\mathbb{I}_1 := \left(\frac{\mathbb{I}_{\mathbf{y}} - \mathbb{I}_{\mathbf{z}}}{\mathbb{I}_{\mathbf{x}}}\right), \mathbb{I}_2 := \left(\frac{\mathbb{I}_{\mathbf{z}} - \mathbb{I}_{\mathbf{x}}}{\mathbb{I}_{\mathbf{y}}}\right), \mathbb{I}_3 := \left(\frac{\mathbb{I}_{\mathbf{x}} - \mathbb{I}_{\mathbf{y}}}{\mathbb{I}_{\mathbf{z}}}\right)$, and considering the states and control input as follows:

$$\begin{cases} x_1 = p_{\mathbf{x}}, & x_2 = \dot{p}_{\mathbf{x}}, & x_3 = p_{\mathbf{y}}, & x_4 = \dot{p}_{\mathbf{y}}, \\ x_5 = p_{\mathbf{z}}, & x_6 = \dot{p}_{\mathbf{z}}, & x_7 = \phi, & x_8 = \dot{\phi}, \\ x_9 = \theta, & x_{10} = \dot{\theta}, & x_{11} = \psi, & x_{12} = \dot{\psi}, \end{cases} \quad (3)$$

$$Z(t) := [x_1 \quad x_2 \quad \cdots \quad x_{12}]^T, V(t) := [T \quad \tau_\phi \quad \tau_\theta \quad \tau_\psi]^T,$$

the state-space dynamics of a typical quadrotor can be expressed as:

$$\dot{Z}(t) = \underbrace{\begin{bmatrix} x_2 \\ 0 \\ x_4 \\ 0 \\ x_6 \\ -g \\ x_8 \\ \mathbb{I}_1 x_{10} x_{12} - \frac{J x_{10}\omega_5}{\mathbb{I}_{\mathbf{x}}} \\ x_{10} \\ \mathbb{I}_2 x_8 x_{12} + \frac{J x_8 \omega_5}{\mathbb{I}_{\mathbf{y}}} \\ x_{12} \\ \mathbb{I}_3 x_8 x_{10} \end{bmatrix}}_{\widehat{f}(Z(t))} + \underbrace{\begin{bmatrix} 0 & 0 & 0 & 0 \\ \frac{q_1}{m} & 0 & 0 & 0 \\ 0 & 0 & 0 & 0 \\ \frac{q_2}{m} & 0 & 0 & 0 \\ 0 & 0 & 0 & 0 \\ \frac{q_3}{m} & 0 & 0 & 0 \\ 0 & 0 & 0 & 0 \\ 0 & \frac{1}{\mathbb{I}_{\mathbf{x}}} & 0 & 0 \\ 0 & 0 & 0 & 0 \\ 0 & 0 & \frac{1}{\mathbb{I}_{\mathbf{y}}} & 0 \\ 0 & 0 & 0 & 0 \\ 0 & 0 & 0 & \frac{1}{\mathbb{I}_{\mathbf{z}}} \end{bmatrix}}_{\widehat{B}} V(t), \quad (4)$$

where $q_1 := \mathbf{c}_{x_7}\mathbf{c}_{x_{11}}\mathbf{s}_{x_9} + \mathbf{s}_{x_7}\mathbf{s}_{x_{11}}$, $q_2 := \mathbf{c}_{x_7}\mathbf{s}_{x_9}\mathbf{s}_{x_{11}} - \mathbf{c}_{x_{11}}\mathbf{s}_{x_7}$, and $q_3 := \mathbf{c}_{x_9}\mathbf{c}_{x_7}$.

To incorporate the rotor dynamics explicitly, the rotor speeds can be treated as additional system states. Augmenting the states in Eq. (3) with:

$$x_{13} = \omega_1, \quad x_{14} = \omega_2, \quad x_{15} = \omega_3, \quad x_{16} = \omega_4 \quad (5)$$

and defining control input as $U(t) := [\alpha_1 \quad \alpha_2 \quad \alpha_3 \quad \alpha_4]^T$ the overall system dynamics can be rewritten as:

$$\dot{X}(t) = \underbrace{\begin{bmatrix} x_2 \\ \frac{(\mathbf{c}_{x_7}\mathbf{c}_{x_{11}}\mathbf{s}_{x_9} + \mathbf{s}_{x_7}\mathbf{s}_{x_{11}})T}{m} \\ x_4 \\ \frac{(\mathbf{c}_{x_7}\mathbf{s}_{x_9}\mathbf{s}_{x_{11}} - \mathbf{c}_{x_{11}}\mathbf{s}_{x_7})T}{m} \\ x_6 \\ -g + \frac{(\mathbf{c}_{x_9}\mathbf{c}_{x_7})T}{m} \\ x_8 \\ \mathbb{I}_1 x_{10} x_{12} - \frac{J x_{10}\omega_5}{\mathbb{I}_{\mathbf{x}}} + \frac{\tau_\phi}{\mathbb{I}_{\mathbf{x}}} \\ x_{10} \\ \mathbb{I}_2 x_8 x_{12} + \frac{J x_8 \omega_5}{\mathbb{I}_{\mathbf{y}}} + \frac{\tau_\theta}{\mathbb{I}_{\mathbf{y}}} \\ x_{12} \\ \mathbb{I}_3 x_8 x_{10} + \frac{\tau_\psi}{\mathbb{I}_{\mathbf{z}}} \\ 0 \\ 0 \\ 0 \\ 0 \end{bmatrix}}_{f(X(t))} + \underbrace{\begin{bmatrix} \mathbf{0}_{12 \times 4} \\ \mathbf{I}_{4 \times 4} \end{bmatrix}}_{B} U(t), \quad (6)$$

where $X(t) := \begin{bmatrix} Z(t)^T & x_{13} & x_{14} & x_{15} & x_{16} \end{bmatrix}^T$, $\omega_5 := \sum_{i=13}^{16} (-1)^{i+1} x_i$.

In the next section, we utilize both the state-space formulations presented in Eq. (4) and Eq. (6) to formulate OCPs aimed at generating least-energy trajectories. To proceed, we introduce the following definitions:

Definition 1 (Mission): A quadrotor mission $\mathbb{M}(\mathbf{x}_i \mathbf{y}_j \mathbf{z}_k)$ is defined as a flight from co-ordinates $(0,0,0)$ to (i,j,k) (in metres) along the inertial $\mathbf{x}$, $\mathbf{y}$ and $\mathbf{z}$ axes, respectively.

Definition 2 (Trajectory): A trajectory $\mathbb{T}_{\mathbb{M}(\mathbf{x}_i \mathbf{y}_j \mathbf{z}_k)} := \{\mathbf{x}_i(t), \mathbf{y}_j(t), \mathbf{z}_k(t)\}$ is a set containing the time parameterized path taken by the quadrotor to complete a mission $\mathbb{M}(\mathbf{x}_i \mathbf{y}_j \mathbf{z}_k)$. Here, $\mathbf{x}_i(t), \mathbf{y}_j(t), \mathbf{z}_k(t)$ are the positions of the quadrotor with respect to time.

There are infinitely many trajectories between $(0,0,0)$ and (i,j,k). The objective of this work is to identify at least one

optimal trajectory where the energy consumption is the least. To calculate the energy consumed in following a trajectory we need the energy consumption model of a quadrotor which is discussed next.

C. Energy consumption model

As highlighted in the introduction, we adopt a physics-based approach [7] to develop the ECM for a quadrotor. In this formulation, we make the following assumptions:

Assumption 1: Most of a quadrotor's energy consumption is due to the rotors, with the energy used by navigation, communication, and other subsystems being negligible [3]. Further, energy losses from the ESC, battery inefficiencies, and the absence of a gearbox between the motor and propeller are neglected.

Assumption 2: In simulations, there is no physical ground to prevent a free fall, so hover conditions are enforced at the start and end. Hence, it is assumed that for $k \in \{1, 2, 3, 4\}$, $\Omega_k(t_0) = \Omega_k(t_f) = \Omega_h$, ($\Omega_h$ is the angular velocity during hover) i.e., the initial and final angular velocities of each motor are equal [7][1].

Based on the rotor speeds and acceleration of a quadrotor, the total energy E_M consumed by the quadrotor between $[t_i, t_f]$ is given by [7], [11]

$$
E_M = \int_{t_0}^{t_f} \left[\sum_{i=1}^{4} \left\{ c_1 + c_2\omega_i(t) + c_3\omega_i^2(t) + c_4\omega_i^3(t) + \\ c_5\omega_i^4(t) + c_6\alpha_i^2(t) \right\} \right] dt \quad (7)
$$

where c_1, c_2, c_3, c_4, c_5, and c_6 are constants that explicitly depends on the motor and propeller specifications.

In this work, we perform the numerical simulations on two different quadrotor systems namely, $\mathbb{Q}_1$ and $\mathbb{Q}_2$ whose parameters are derived from [7] and [10], respectively. The constants $c_1, c_2, \cdots, c_6$ and other physical parameters for each of the quadrotors are listed in Table I. In the following section, we employ the ECM from Eq. (7) to formulate the OCP.

Quadrotor $\mathbb{Q}_1$		
$m = 1.3\ kg$	$d = 0.175\ m$	$J = 3.9 \times 10^{-5}\ kgm^2$
$\mathbb{I}_x = 0.081\ kgm^2$	$\mathbb{I}_y = 0.081\ kgm^2$	$\mathbb{I}_z = 0.142\ kgm^2$
$c_1 = 2.9702\ W$	$c_2 = 0.069702\ W/(rad/s)$	$c_3 = 0.0002776\ W/(rad/s)^2$
$c_4 = 3.924 \times 10^{-8}\ W/(rad/s)^3$	$c_5 = 9.413 \times 10^{-13}\ W/(rad/s)^4$	$c_6 = 3.259 \times 10^{-6}\ W/(rad/s^2)^2$
$\kappa_T = 3.8305 \times 10^{-6}\ Ns^2/rad^2$	$\kappa_\tau = 2.2518 \times 10^{-8}\ Nms^2/rad^2$	$\mathtt{U}_{\omega_i} = 1047.19\ rad/s$
$\mathtt{L}_{\alpha_i} = -1000\ rad/s^2$	$\mathtt{U}_{\alpha_i} = 1000\ rad/s^2$	$\omega_{h_i} = 912.11\ rad/s$
$\mathtt{U}_{x_2} = \mathtt{U}_{x_4} = 15\ m/s$ $\mathtt{L}_{x_2} = \mathtt{L}_{x_4} = -15\ m/s$	$\mathtt{U}_{x_6} = 6\ m/s$ $\mathtt{L}_{x_6} = -2\ m/s$	$\mathtt{U}_{x_{11}} = \pi\ rad$ $\mathtt{L}_{x_{11}} = -\pi\ rad$
$\mathtt{U}_{x_7} = \mathtt{U}_{x_9} = 35 \times \frac{\pi}{180}\ rad$ $\mathtt{L}_{x_7} = \mathtt{L}_{x_9} = -35 \times \frac{\pi}{180}\ rad$	$\mathtt{U}_{x_8} = \mathtt{U}_{x_{10}} = 1.5\ rad/s$ $\mathtt{L}_{x_8} = \mathtt{L}_{x_{10}} = -1.5\ rad/s$	$\mathtt{U}_{x_{12}} = 1.5\ rad/s$ $\mathtt{L}_{x_{12}} = -1.5\ rad/s$
Quadrotor $\mathbb{Q}_2$		
$m = 3\ kg$	$d = 0.3\ m$	$J = 8.02 \times 10^{-4}\ kgm^2$
$\mathbb{I}_x = 0.0429\ kgm^2$	$\mathbb{I}_y = 0.0429\ kgm^2$	$\mathbb{I}_z = 0.077\ kgm^2$
$c_1 = 1.12\ W$	$c_2 = 0.0527\ W/(rad/s)$	$c_3 = 0.00027281\ W/(rad/s)^2$
$c_4 = 1.115 \times 10^{-6}\ W/(rad/s)^3$	$c_5 = 5.019 \times 10^{-10}\ W/(rad/s)^4$	$c_6 = 0.00040838\ W/(rad/s^2)^2$
$\kappa_T = 4.848 \times 10^{-5}\ Ns^2/rad^2$	$\kappa_\tau = 8.891 \times 10^{-7}\ Nms^2/rad^2$	$\mathtt{U}_{\omega_i} = 640\ rad/s$
$\mathtt{L}_{\alpha_i} = -600\ rad/s^2$	$\mathtt{U}_{\alpha_i} = 600\ rad/s^2$	$\omega_{h_i} = 389.50\ rad/s$
$\mathtt{U}_{x_2} = \mathtt{U}_{x_4} = 20\ m/s$ $\mathtt{L}_{x_2} = \mathtt{L}_{x_4} = -20\ m/s$	$\mathtt{U}_{x_6} = 10\ m/s$ $\mathtt{L}_{x_6} = -8\ m/s$	$\mathtt{U}_{x_{11}} = \pi\ rad$ $\mathtt{L}_{x_{11}} = -\pi\ rad$
$\mathtt{U}_{x_7} = \mathtt{U}_{x_9} = 1\ rad$ $\mathtt{L}_{x_7} = \mathtt{L}_{x_9} = -1\ rad$	$\mathtt{U}_{x_8} = \mathtt{U}_{x_{10}} = 1\ rad/s$ $\mathtt{L}_{x_8} = \mathtt{L}_{x_{10}} = -1\ rad/s$	$\mathtt{U}_{x_{12}} = 1\ rad/s$ $\mathtt{L}_{x_{12}} = -1\ rad/s$

TABLE I: Quadrotor parameters with $i \in \{1, 2, 3, 4\}$

III. OCP FORMULATION AND SOLUTION

This section formulates the OCP for least-energy trajectory generation and presents simulation results, along with a comparative analysis against a state-of-the-art method. The state-of-the-art OCP (defined in Section III-C) is based on the state

---

space representation given in Eq. (4) and the one that we use is based on Eq. (6).

A. Problem statement

Consider a quadrotor $\mathbb{Q}$ with dynamics as given in Eq. (6). Let $\mathbb{M}(\mathbf{x}_i\mathbf{y}_j\mathbf{z}_k)$ be a mission $\mathbb{Q}$ needs to complete. Then find an admissible input $U(t)$ and time $t_f \in \mathbb{R}$ such that the following OCP is solved:

OCP-I objective:

$$
\min_{U(t), t_f} \mathbb{E}_{\mathbb{M}(\mathbf{x}_i\mathbf{y}_j\mathbf{z}_k)}
$$

$$
= \min_{U(t), t_f} \int_{t_0}^{t_f} \left[\sum_{i=13}^{i=16} \left\{ c_1 + c_2 x_i(t) + c_3 x_i^2(t) + c_4 x_i^3(t) \right. \right.
$$

$$
\left. \left. + c_5 x_i^4(t) \right\} + c_6 \sum_{j=1}^{4} \alpha_j^2(t) \right] dt \quad (8)
$$

OCP-I constraints:

System dynamics:	$\dot{X}(t) = f(X(t)) + BU(t)$
State constraints:	$\mathtt{L}_X < X(t) < \mathtt{U}_X$
Input constraints:	$\mathtt{L}_U < U(t) < \mathtt{U}_U$
Boundary conditions:	$X(t_i) = X_{t_i}, X(t_f) = X_{t_f}$

Solving the above OCP yields the optimal input $U^*(t)$ and optimal mission time $t^*_{\mathbb{M}(\mathbf{x}_i\mathbf{y}_j\mathbf{z}_k)}$ for quadrotor $\mathbb{Q}$ to complete mission $\mathbb{M}(\mathbf{x}_i\mathbf{y}_j\mathbf{z}_k)$ with optimal (least) energy $\mathbb{E}^*_{\mathbb{M}(\mathbf{x}_i\mathbf{y}_j\mathbf{z}_k)}$. Using these, the optimal state $X^*(t)$ and the least-energy trajectory $\mathbb{T}^*_{\mathbb{M}(\mathbf{x}_i\mathbf{y}_j\mathbf{z}_k)} = \{x_1^*(t), x_3^*(t), x_5^*(t)\}$ are computed. The energy consumed in a quadrotor mission consists of hover energy (to counter weight) and propulsion energy (for maneuver). Mission time t_f affects this balance where a large t_f increases hover energy, whereas, a small t_f increases propulsion energy. To optimize this trade-off, we use a free final time in our OCP, unlike many works that fixes it arbitrarily [7]. We now present numerical simulations of the OCP solution for various missions using two quadrotors, $\mathbb{Q}_1$ and $\mathbb{Q}_2$.

B. Numerical Simulations

The simulations were carried out on an Intel Core i7 computer at 2.90 GHz with 32 GB RAM using Windows 11 Pro operating system. The OCP in Section III-A is solved numerically using optimal control solver GPOPS-II coupled with a nonlinear programming solver Interior Point OPTimizer (IPOPT) [12]. We present the simulation results for the following four missions.

- Mission $\mathbb{M}_1 := \mathbb{M}(\mathbf{x}_{00}\mathbf{y}_{00}\mathbf{z}_{25})$ involves a 1D flight with motion restricted to $\mathbf{z}$ axis.
- Missions $\mathbb{M}_2 := \mathbb{M}(\mathbf{x}_{20}\mathbf{y}_{00}\mathbf{z}_{30})$ and $\mathbb{M}_3 := \mathbb{M}(\mathbf{x}_{30}\mathbf{y}_{00}\mathbf{z}_{20})$ are 2D flights along the $\mathbf{x}$-$\mathbf{z}$ plane, where $\mathbb{M}_2$ follows the condition $x(t_f) < z(t_f)$ and $\mathbb{M}_3$ follows $x(t_f) > z(t_f)$.
- Mission $\mathbb{M}_4 := \mathbb{M}(\mathbf{x}_{40}\mathbf{y}_{30}\mathbf{z}_{20})$ represents a 3D flight scenario.

For each mission $\mathbb{M}(\mathbf{x}_i\mathbf{y}_j\mathbf{z}_k)$, we define the boundary constraints, state constraints and input constraints (refer Table II) and invoke the solver to obtain the optimal input, time, states, trajectory, and energy, i.e., $U^*(t)$, $t^*_{\mathbb{M}(\mathbf{x}_i\mathbf{y}_j\mathbf{z}_k)}$, $X^*(t)$, $\mathbb{T}^*_{\mathbb{M}(\mathbf{x}_i\mathbf{y}_j\mathbf{z}_k)}$, and $\mathbb{E}^*_{\mathbb{M}(\mathbf{x}_i\mathbf{y}_j\mathbf{z}_k)}$, respectively. The numerical simulations are performed using attributes of both $\mathbb{Q}_1$ and $\mathbb{Q}_2$ as given in Table I.

The optimal trajectories for all four missions are depicted in 3D in Fig. 2, illustrating how the physical characteristics of the quadrotor influence the least-energy flight trajectories. Further, a side-by-side comparison of the least-energy trajectories for

---

[1]Using hover-to-hover missions has become a standard benchmark in academic research and simulations. It provides a controlled way to compare different planning or control methods on an equal footing.

Particulars	Quadrotor $\mathbb{Q}_1$	Quadrotor $\mathbb{Q}_2$
State constraints	$L_X = [\mathbf{1}_2 \otimes [0 \quad -10] \quad 0 \quad -2 \quad \mathbf{1}_2 \otimes [-35 \times \frac{\pi}{180} \quad -1.5] \quad -\pi \quad -1.5 \quad 0 \times \mathbf{1}_4]^T$ $U_X = [\mathbf{1}_2 \otimes [60 \quad 10] \quad 40 \quad 6 \quad [\mathbf{1}_2 \otimes 35 \times \frac{\pi}{180} \quad 1.5] \quad \pi \quad 1.5 \quad 1047.19 \times \mathbf{1}_4]^T$	$L_X = [\mathbf{1}_2 \otimes [0 \quad -20] \quad 0 \quad -8 \quad \mathbf{1}_2 \otimes [-1 \quad -1] \quad -\pi \quad -1 \quad 0 \times \mathbf{1}_4]^T$ $U_X = [\mathbf{1}_2 \otimes [60 \quad 20] \quad 40 \quad 10 \quad \mathbf{1}_2 \otimes [1 \quad 1] \quad \pi \quad 1 \quad 640 \times \mathbf{1}_4]^T$
Input constraints	$L_U = [-1000 \times \mathbf{1}_4]^T$ $U_U = [1000 \times \mathbf{1}_4]^T$	$L_U = [-600 \times \mathbf{1}_4]^T$ $U_U = [600 \times \mathbf{1}_4]^T$
Boundary conditions	$X_{t_i} = [0 \times \mathbf{1}_{12} \quad \omega_h \times \mathbf{1}_4]^T$ $X_{t_f} = [i \quad 0 \quad j \quad 0 \quad k \quad 0 \quad 0 \times \mathbf{1}_6 \quad \omega_h \times \mathbf{1}_4]^T$, $\omega_h = 912.11$	$X_{t_i} = [0 \times \mathbf{1}_9 \quad \omega_h \times \mathbf{1}_4]^T$ $X_{t_f} = [i \quad 0 \quad j \quad 0 \quad k \quad 0 \quad 0 \times \mathbf{1}_6 \quad \omega_h \times \mathbf{1}_4]^T$, $\omega_h = 389.5$

TABLE II: State and input constraints with boundary conditions for mission $\mathbb{M}(\mathbf{x}_i \mathbf{y}_j \mathbf{z}_k)$

mission $\mathbb{M}_4$ using quadrotors $\mathbb{Q}_1$ and $\mathbb{Q}_2$ is also presented in Fig. 3 which illustrates that the least energy trajectory for $\mathbb{Q}_1$ and $\mathbb{Q}_2$ are different.
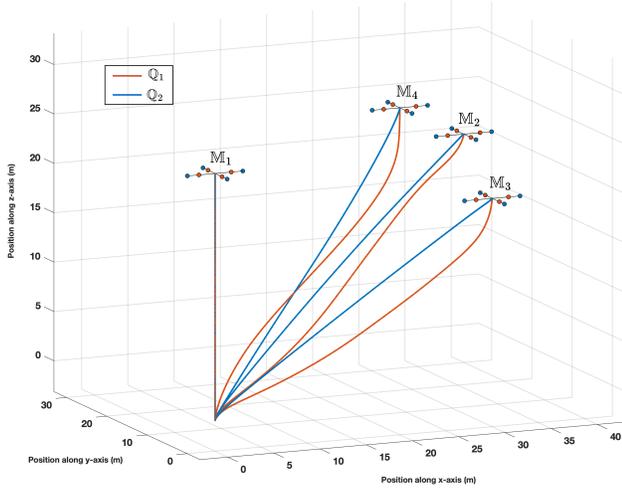
Fig. 2: Optimal paths for $\mathbb{M}_1$, $\mathbb{M}_2$, $\mathbb{M}_3$, $\mathbb{M}_4$ with $\mathbb{Q}_1$ and $\mathbb{Q}_2$
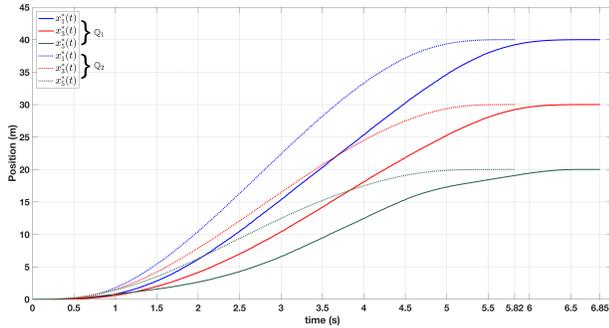
Fig. 3: Optimal position trajectory for $\mathbb{M}_4$ on $\mathbb{Q}_1$ and $\mathbb{Q}_2$

For mission $\mathbb{M}_4$, quadrotor $\mathbb{Q}_1$ would need a minimum of 9896.8 J ($\mathbb{E}^*_{\mathbb{M}_4}$) energy with an optimal flight time $t^*_{\mathbb{M}_4} = 6.9$ s, while $\mathbb{Q}_2$ can complete the same mission with a reduced energy consumption of $\mathbb{E}^*_{\mathbb{M}_4} = 4135.9$ J and an optimal flight time of $t^*_{\mathbb{M}_4} = 5.8$ s. This result highlights the critical influence of quadrotor parameters on energy efficiency. Fig. 4 display the optimal states and control inputs plots for missions $\mathbb{M}_4$ on quadrotor $\mathbb{Q}_1$. Similar plots and comparisons can be made for other missions as well, but they are not included in this paper for the sake of conciseness. Table III enumerates the least energy and optimal mission time requirement of $\mathbb{Q}_1$ and $\mathbb{Q}_2$ for missions $\mathbb{M}_1$, $\mathbb{M}_2$, $\mathbb{M}_3$, $\mathbb{M}_4$.

The next subsection underscores the significance of selecting rotor acceleration as the control input for solving the OCP.

C. Importance of rotor acceleration as input of the OCP

In the literature, OCPs similar to that described in Section III-A are typically formulated using thrusts and torques as control inputs [10]. However, such control inputs present their own set of challenges. This section aims to highlight these issues and validate them by comparing the solution of the

Mission	Quadrotor $\mathbb{Q}_1$		Quadrotor $\mathbb{Q}_2$	
$\mathbb{M}_i$	$\mathbb{E}^*_{\mathbb{M}_i}$ [J]	$t^*_{\mathbb{M}_i}$ [s]	$\mathbb{E}^*_{\mathbb{M}_i}$ [J]	$t^*_{\mathbb{M}_i}$ [s]
$\mathbb{M}_1 := \mathbb{M}(\mathbf{x}_{00}\mathbf{y}_{00}\mathbf{z}_{25})$	7624.0	5.8	2817.6	4.2
$\mathbb{M}_2 := \mathbb{M}(\mathbf{x}_{20}\mathbf{y}_{00}\mathbf{z}_{30})$	9079.1	6.7	3364.3	5.0
$\mathbb{M}_3 := \mathbb{M}(\mathbf{x}_{30}\mathbf{y}_{00}\mathbf{z}_{20})$	8507.4	6.0	3476.6	5.0
$\mathbb{M}_4 := \mathbb{M}(\mathbf{x}_{40}\mathbf{y}_{30}\mathbf{z}_{20})$	9896.8	6.9	4135.9	5.8

TABLE III: Least energy and optimal mission time requirement of $\mathbb{Q}_1$ and $\mathbb{Q}_2$ for various missions

OCP in Section III-A with that presented in [10]. For clarity, we reformulate the OCP from [10] next and refer to it as *OCP-II*, while labeling the the problem in Section III-A as *OCP-I*.

OCP-II objective:

$$\min_{V(t),t_f} \mathbb{E}_{\mathbb{M}(\mathbf{x}_i\mathbf{y}_j\mathbf{z}_k)}$$
$$= \min_{V(t),t_f} \int_{t_0}^{t_f} \left[\sum_{i=1}^{i=4} \left\{ c_1 + c_2\omega_i(t) + c_3\omega_i^2(t) + c_4\omega_i^3(t) + c_5\omega_i^4(t) \right\} \right] dt \tag{9}$$

OCP-II constraints:

System dynamics:	$\dot{Z}(t) = \widehat{f}(Z(t)) + \widehat{B}U(t)$
State constraints:	$L_Z < Z(t) < U_Z$
Input constraints:	$0 < T(t) < U_T = 4\kappa_T U_\omega^2$
	$0 < \tau_j < U_{\tau_j}, j \in \{\phi, \theta, \psi\}$
Boundary conditions:	$X(t_i) = X_{t_i}, X(t_f) = X_{t_f}$

Note that *OCP-I* and *OCP-II* share a similar structure, except for the choice of control inputs. In *OCP-I*, the objective functional is minimized over the rotor acceleration $U(t)$ and final time t_f, whereas in *OCP-II*, the optimization is performed over the thrust and suitable torques $V(t)$ and t_f. Furthermore, the objective integrand in *OCP-II* does not explicitly include the rotor accelerations. As a result, one of the limitations of *OCP-II* is its reduced fidelity in minimizing energy consumption, since it is an important contributor to energy usage, as evident from Eq. (7).

Further note that although *OCP-II* imposes constraints on thrust (T) and torques ($\tau_\phi, \tau_\theta, \tau_\psi$), it does not consider limitations on their rate of change. In practice, however, abrupt changes in thrust or torque—which a solver might otherwise request to accomplish a mission objective—are naturally prevented by physical constraints on rotor speeds and accelerations. The next theorem formally establishes the constraints on the rate of thrust and torque generated by the rotors of a quadrotor. Additionally, since the rotors cannot reverse their spin, it is reasonable to assume without loss of generality that $L_{\omega_i} \geq 0$. In contrast, angular acceleration can indeed become negative during rotor deceleration, enabling the assumption that $L_{\alpha_i} < 0$ (Here, $i \in \{1, 2, 3, 4\}$).

Theorem 1: Let $\omega_i(t), \alpha_i(t), \tau_\phi, \tau_\theta, \tau_\psi$ be as defined in Section II-A. Let T_i be the thrust from each rotors, where $i \in \{1, 2, 3, 4\}$ and T be the total thrust. Assume $\omega_i \in [L_{\omega_i}, U_{\omega_i}]$ and $\alpha_i \in [L_{\alpha_i}, U_{\alpha_i}]$, where $L_{\omega_i} \geq 0, U_{\omega_i} > 0, L_{\alpha_i} < 0, U_{\alpha_i} > 0$
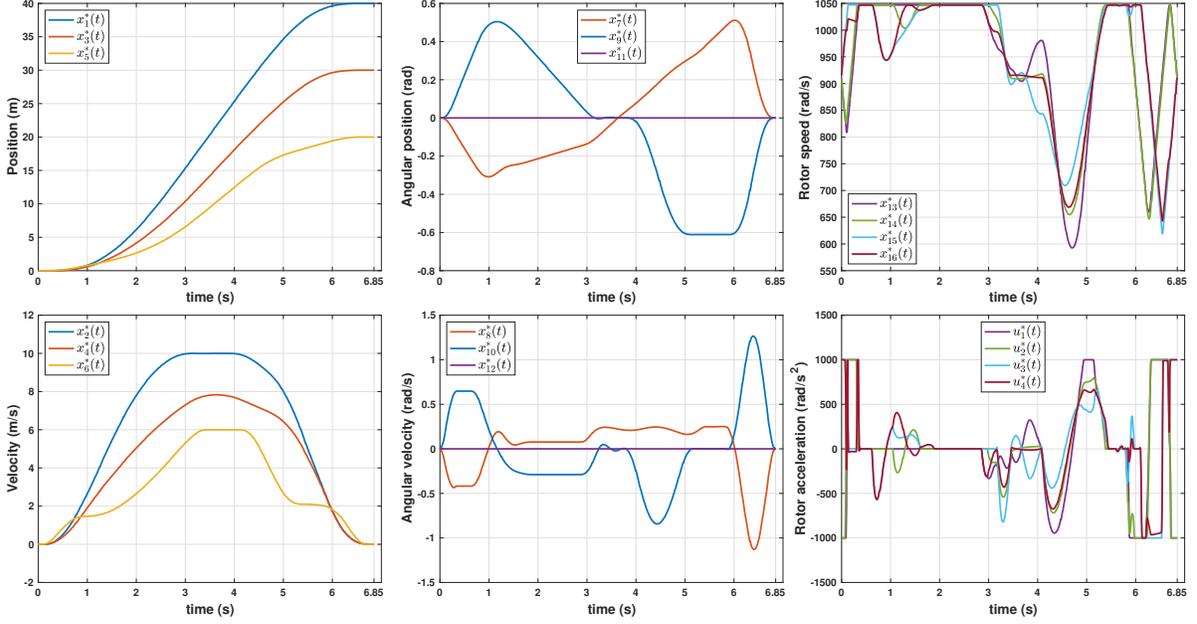
Fig. 4: Optimal state and control plots for $\mathbb{M}_4$ on $\mathbb{Q}_1$

for all $i \in \{1, 2, 3, 4\}$. Then thrust and torques on are bounded as follows:

1) $\kappa_T \sum_{i=1}^4 \mathtt{L}_{\omega_i}^2 \leqslant T \leqslant \kappa_T \sum_{i=1}^4 \mathtt{U}_{\omega_i}^2$.
2) $d \times \kappa_T(\mathtt{L}_{\omega_4}^2 - \mathtt{U}_{\omega_2}^2) \leqslant \tau_\phi \leqslant d \times \kappa_T(\mathtt{U}_{\omega_4}^2 - \mathtt{L}_{\omega_2}^2)$
3) $d \times \kappa_T(\mathtt{L}_{\omega_3}^2 - \mathtt{U}_{\omega_1}^2) \leqslant \tau_\theta \leqslant d \times \kappa_T(\mathtt{U}_{\omega_3}^2 - \mathtt{L}_{\omega_1}^2)$
4) $-\kappa_\tau(\mathtt{L}_{\omega_2}^2 + \mathtt{L}_{\omega_4}^2) \leqslant \tau_\psi \leqslant \kappa_\tau(\mathtt{L}_{\omega_1}^2 + \mathtt{L}_{\omega_3}^2)$

Further, the thrust and torque rates are bounded as follows:

1) $\sum_{i=1}^4 \mathtt{U}_{\omega_i} \mathtt{L}_{\alpha_i} \leqslant \dfrac{\dot{T}}{2 \times \kappa_T} \leqslant \sum_{i=1}^4 \mathtt{U}_{\omega_i} \mathtt{U}_{\alpha_i}$

2) $\mathtt{U}_{\omega_4} \mathtt{L}_{\alpha_4} - \mathtt{U}_{\omega_2} \mathtt{U}_{\alpha_2} \leq \dfrac{\dot{\tau}_\phi}{2d \times \kappa_T} \leq \mathtt{U}_{\omega_4} \mathtt{U}_{\alpha_4} - \mathtt{U}_{\omega_2} \mathtt{L}_{\alpha_2}$

3) $\mathtt{U}_{\omega_3} \mathtt{L}_{\alpha_3} - \mathtt{U}_{\omega_1} \mathtt{U}_{\alpha_1} \leq \dfrac{\dot{\tau}_\theta}{2d \times \kappa_T} \leq \mathtt{U}_{\omega_3} \mathtt{U}_{\alpha_3} - \mathtt{U}_{\omega_1} \mathtt{L}_{\alpha_1}$

4) $\mathtt{U}_{\Omega_1} \mathtt{L}_{\alpha_1} - \mathtt{U}_{\Omega_2} \mathtt{U}_{\alpha_2} + \mathtt{U}_{\Omega_3} \mathtt{L}_{\alpha_3} - \mathtt{U}_{\Omega_4} \mathtt{U}_{\alpha_4} \leqslant \dfrac{\dot{\tau}_\psi}{2\kappa_\tau} \leqslant$
$\mathtt{U}_{\Omega_1} \mathtt{U}_{\alpha_1} - \mathtt{U}_{\Omega_2} \mathtt{L}_{\alpha_2} + \mathtt{U}_{\Omega_3} \mathtt{U}_{\alpha_3} - \mathtt{U}_{\Omega_4} \mathtt{L}_{\alpha_4}$

Proof: The proofs of the statements follow directly from Eq. (1) and Eq. (2), and are omitted here due to space constraints. ∎

From Theorem 1 it is evident that the limits on net thrust T and its rate $\dot{T}$ depends on the upper and lower limits of rotor speed and rotor acceleration. Hence, in *OCP-I*, the rate constraints from Theorem 1 are implicitly enforced through limits on rotor speed (state constraints) and rotor acceleration (input constraints). By including angular acceleration as a control input, *OCP-I* enables direct constraints on $\dot{T}$. In contrast, *OCP-II* lacks a mechanism to explicitly constrain angular acceleration.

Another challenge with *OCP-II* is that the formulation may permit angular accelerations and rotor speeds to exceed their practical limits. In this case, the solver optimizes thrust and torques independently, subject to their respective bounds, without directly considering the relation in Eq. (2). After solving for the optimal thrust and torques, rotor speeds are computed using Eq. (2). For example, consider the case where $T = \mathtt{U}_T$ (i.e., maximum thrust is requested by the solver) and using the relation $\mathtt{U}_{\omega_3} = \sqrt{\frac{\mathtt{U}_T}{4\kappa_T}}$ (based on $\mathtt{U}_{\omega_i} = \mathtt{U}_\omega$ for all $i \in 1, 2, 3, 4$ and $\mathtt{U}_T = 4\kappa_T \mathtt{U}_\omega^2$), it can be shown from Eq. (2) that $\omega_3 > \mathtt{U}_\omega$ when τ_θ and τ_ψ are positive. Therefore, the rotor speeds can go beyond their bounds. In contrast, *OCP-I* effectively addresses this limitation as the solver can only choose rotor speeds that are bounded. Using Theorem 1 and Table I, for $\mathbb{Q}_1$, we have, $\mathtt{L}_T = 0$, $\mathtt{U}_T = 16.79$, $\mathtt{L}_{\dot{T}} = -32.08$, $\mathtt{U}_{\dot{T}} = 32.08$, $\mathtt{L}_{\tau_j} = -0.73$, $\mathtt{U}_{\tau_j} = 0.73$, $\mathtt{L}_{\dot{\tau}_j} = -2.81$, $\mathtt{U}_{\dot{\tau}_j} = 2.81$, $(j \in \{\phi, \theta\})$.

In order to highlight the limitations of *OCP-II*, we compare solutions of *OCP-I* and *OCP-II* for Mission $\mathbb{M}_4$, by taking $\mathbb{Q}_1$. The *OCP-II* formulation yields $\mathbb{E}_{\mathbb{M}_4}^* = 9346.9$ J and $t_{\mathbb{M}_4}^* = 6.5$ s. The lower energy and time values under *OCP-II* can be attributed to the absence of constraints on the rate of change of rotor speeds, allowing $T(t), \tau_\phi(t), \tau_\theta(t), \tau_\psi(t)$ to vary almost instantaneously. Furthermore, simulation results for the optimal states, optimal inputs along with rotor speed and rotor acceleration for $\mathbb{M}_4$ using *OCP-II* shown in Fig. 5 demonstrates that with *OCP-II*, rotor speed and angular acceleration exceeds $\mathtt{U}_\omega$ and $\mathtt{L}_\alpha$, $\mathtt{U}_\alpha$. We also show the variation of T and $\dot{T}$ for *OCP-II* in Fig. 5. From the plots, we can see that $\dot{T}$ exceeds the bounds in *OCP-II*.

Consequently, *OCP-II* (or any OCP formulation with thrust T and torque as inputs) can encounter these issues unless explicit bounds on rotor speeds and rotor accelerations are incorporated into the problem formulation. By contrast, *OCP-I* prevents this issue by explicitly modeling rotor speed as state and rotor acceleration as an input, thereby allowing direct constraints on these quantities. Thrust T and torques are then computed using Eq. (1), ensuring all constraints are satisfied. In the next subsection we discuss how optimal energy consumption ($\mathbb{E}_\mathbb{M}^*$) varies with maximum value of rotor speed ($\mathtt{U}_\omega$) and rotor acceleration ($\mathtt{U}_\alpha$).

D. Variation of optimal energy consumption with maximum rotor speed and maximum rotor acceleration

In order to show the variation of optimal energy consumption ($\mathbb{E}_\mathbb{M}^*$) with maximum rotor speed ($\mathtt{U}_\omega$), we consider different values of $\mathtt{U}_\omega$ and solve *OCP-I* for all of the missions mentioned in Section III-B. The values of $\mathbb{E}_{\mathbb{M}_i}^*$ along with $t_{\mathbb{M}_i}^*$ for $\mathbb{Q}_1$ are populated in Figure 6. It is observed that both $\mathbb{E}_{\mathbb{M}_i}^*$ and $t_{\mathbb{M}_i}^*$ reduces with increasing values of $\mathtt{U}_\omega$ upto a point beyond which it gets stalled. Similar trend is noted with the
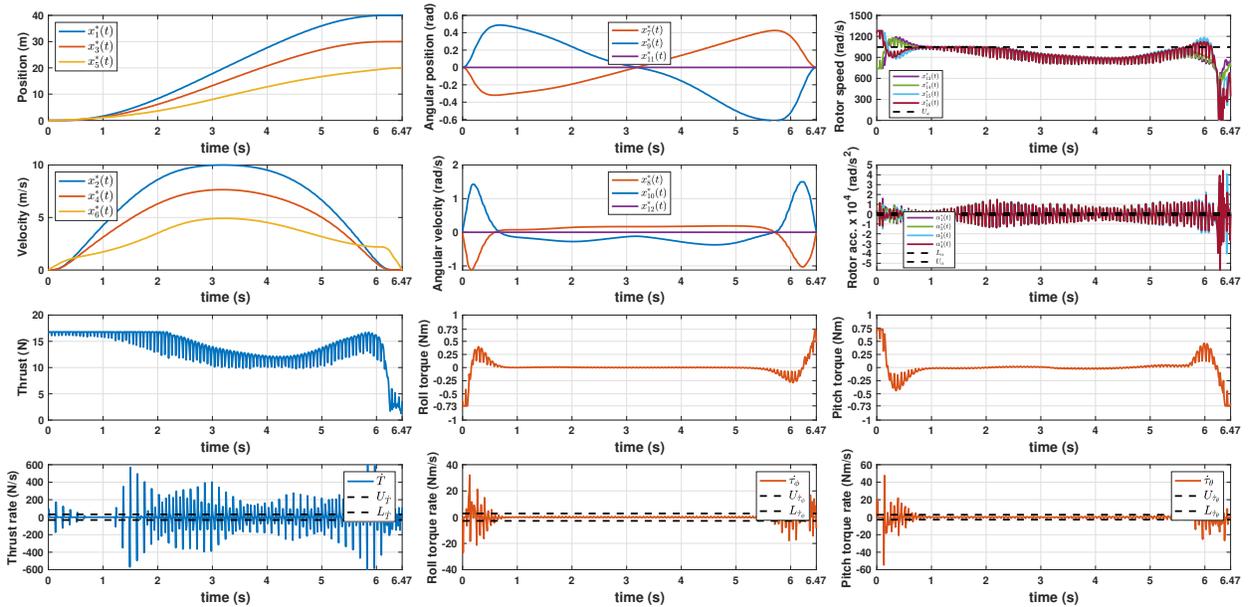
Fig. 5: Optimal state and inputs for $\mathbb{Q}_1$ to complete $\mathbb{M}_4$ found using *OCP-II*

variation of $\mathbb{E}_{\mathbb{M}_i}^*$ and $t_{\mathbb{M}_i}^*$ with $\mathtt{U}_\alpha$ (refer Figure 7), however, the reduction is not as significant like that with $\mathtt{U}_\omega$. Note that similar results are seen for $\mathbb{Q}_2$ but are not included in this paper for conciseness. These data suggest that selecting appropriate rotor hardware can further optimize energy consumption.
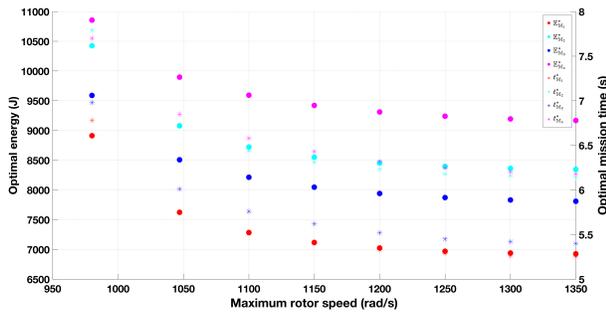

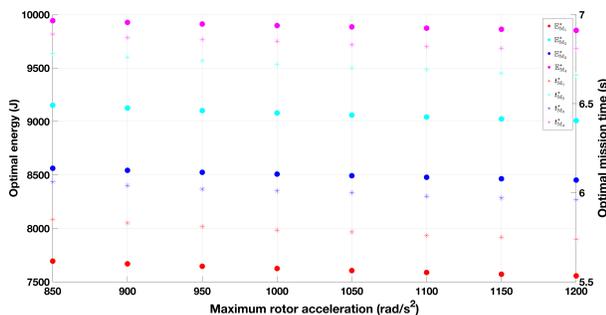Fig. 6: Variation of $\mathbb{E}_{\mathbb{M}_i}^*$ and $t_{\mathbb{M}_i}^*$ with $\mathtt{U}_\omega$

Fig. 7: Variation of $\mathbb{E}_{\mathbb{M}_i}^*$ and $t_{\mathbb{M}_i}^*$ with $\mathtt{U}_\alpha$

IV. CONCLUSION

In this work, we formulated an OCP to generate energy-efficient quadrotor trajectories, jointly optimizing the mission time to balance hover and propulsion energy. Unlike prior studies, we demonstrated that using rotor accelerations as control inputs enables the OCP to naturally enforce the quadrotor's physical constraints, as evidenced by a comparison with an OCP based on thrust and torque inputs. Additionally, we show that an appropriate selection of rotor parameters can further reduce total energy consumption. Although the OCP generates trajectories for an open-loop quadrotor system, analyzing the impact of controller tuning on closed-loop energy consumption is left for future work.

REFERENCES

[1] Moad Idrissi, Mohammad Salami, and Fawaz Annaz. A Review of Quadrotor Unmanned Aerial Vehicles: Applications, Architectural Design and Control Algorithms. *Journal of Intelligent and Robotic Systems: Theory and Applications*, 104(2), 2022.

[2] Juan Zhang, James F Campbell, Donald C Sweeney II, and Andrea C Hupman. Energy consumption models for delivery drones: A comparison and assessment. *Transportation Research Part D: Transport and Environment*, 90:102668, 2021.

[3] Mariusz Jacewicz, Marcin Zuagaj, Robert Glebocki, and Przemyslaw Bibik. Quadrotor model for energy consumption analysis. *Energies*, 15(19), 2022.

[4] Fouad Yacef, Nassim Rizoug, Laid Degaa, and Mustapha Hamerlain. Energy-efficiency path planning for quadrotor UAV under wind conditions. In *2020 7th International Conference on Control, Decision and Information Technologies (CoDIT)*, volume 1, pages 1133–1138, 2020.

[5] Yash Mulgaonkar, Michael Whitzer, Brian Morgan, Christopher M Kroninger, Aaron M Harrington, and Vijay Kumar. Power and weight considerations in small, agile quadrotors. In *Micro-and Nanotechnology Sensors, Systems, and Applications VI*, volume 9083, pages 376–391, 2014.

[6] Konstantinos Karydis and Vijay Kumar. Energetics in robotic flight at small scales. *Interface Focus*, 7:20160088, 2017.

[7] Fabio Morbidi, Roel Cano, and David Lara. Minimum-energy path generation for a quadrotor UAV. In *2016 IEEE International Conference on Robotics and Automation (ICRA)*, pages 1492–1498, 2016.

[8] Paraj Ganchaudhuri and Chayan Bhawal. Power consumption of a quadrotor based on maneuvers. In *2023 IEEE Guwahati Subsection Conference (GCON)*, pages 01–06, 2023.

[9] Yong Zeng, Jie Xu, and Rui Zhang. Energy minimization for wireless communication with rotary-wing UAV. *IEEE Transactions on Wireless Communications*, 18(4):2329–2345, 2019.

[10] Bin Li, Qingliang Li, Yong Zeng, Yue Rong, and Rui Zhang. 3D trajectory optimization for energy-efficient UAV communication: A control design perspective. *IEEE Transactions on Wireless Communications*, 21(6):4579–4593, 2021.

[11] Robert Mahony, Vijay Kumar, and Peter Corke. Multirotor aerial vehicles: Modeling, estimation, and control of quadrotor. *IEEE Robotics and Automation Magazine*, 19(3):20–32, 2012.

[12] Michael A. Patterson and Anil V. Rao. GPOPS-II: A MATLAB software for solving multiple-phase optimal control problems using hp-adaptive gaussian quadrature collocation methods and sparse nonlinear programming. *ACM Transactions on Mathematical Software*, 41(1), 2014.